Effect of Alloying Compositions on the Stacking Fault Energy and Elasticity of FeNiCrAlCo and FeNiCrAlCu: A First-principles Study for Fe-based High Entropy Superalloy Design

Farhan Nugraha[1], *Muhammad* Fariz Aulia[1], and *Tria* Laksana Achmad[1*]

[1]Department of Metallurgical Engineering, Institut Teknologi Bandung, 40132 Bandung, Indonesia

Abstract. High Entropy Superalloy (HESA) is a classification of materials with promising properties extensively developed to improve performance, resource sustainability, and cost efficiency in high-temperature applications. The need for computation on HESA is due to its time and cost superiority over experiments while maintaining good accuracy. However, thermodynamic data of some rare elements like Zr has not existed in publications based on a phase diagram calculation. First-principles is then used to investigate further the effect of decreasing Ni while adding Cu and Zr on lattice parameters, elasticity, stacking fault energy (SFE), and electronic structure of Fe-based HESA FeNiCrAlCo and FeNiCrAlCu. Adding Cu increases the SFE and ductility while decreasing Ni and adding Zr decreases the SFE and increases the strength but slightly reduces the ductility. Electronic structure analysis showed that adding Zr increases charge accumulation and decreases density of states, then interatomic bonding weakened, interlayer distance increased, and SFE decreased. The Fe-based HESA design can be optimized by reducing Ni concentration and increasing Cr concentration to decrease SFE to significantly increase strength, ductility, and hardness, especially at high temperatures, or adding Zr to decrease SFE value to the maximum. This study will help develop low-cost high entropy superalloys with desired performance.

1 Background

Superalloy is a high-temperature material that exhibits resistance to mechanical and chemical degradation at temperatures close to its melting point by solid solution strengthening and precipitation strengthening mechanisms[1]. Materials for high-temperature applications have a crucial role in various industries, including power generation, aerospace, and chemical processing[2-4]. With the increasingly high operating temperatures in industry and the demand for longer component life, research and development to obtain materials with a better combination of properties remain ongoing. Another aim is to reduce material costs and improve resource sustainability to become a better choice from an economic point of view[5]. Currently, conventional superalloys are developing by adding refractory elements, such as Mo, Ta, Re, and Ru, to improve mechanical strength[6]. An example of a Ni-base superalloy is CM247LC which has a Ta refractory element content of about 3 wt.%. However, adding specific concentrations of refractory elements in superalloys can also result in reduced performance with increased density, incompatibility with coatings, and significantly increased production costs[7].

Alloying systems evolved from conventional alloying based on one or two main elements into multicomponent alloying, where many elements are mixed in large proportions resulting in high entropy alloys (HEA) with four effects: high entropy effects related to the thermodynamics of complex phase formation, sluggish diffusion related to slow phase transformation kinetics, severe lattice distortion regarding changes in lattice parameters, and the cocktail effect where each constituent contributes to producing extraordinary properties[8]. High entropy alloys are obtained by mixing five or more elements with different (non-equimolar) or equal (equimolar) atomic compositions to form a solid solution[9]. The concept of high entropy alloys allows the development of alloys with infinite combinations. The high entropy concept applied to superalloys results in a new class of materials, namely high entropy super alloys (HESA)[10-12]. High entropy superalloy is the development of high entropy alloys that can make precipitated particles γ' uniformly dispersed in the matrix γ with high entropy ($\Delta S_{mix} > 1.5R$) to obtain a strengthening mechanism of precipitates (precipitation strengthening)[13]. This material gains high interest in developing advanced materials due to its unique combination of high strength, high ductility, and good stability at high temperatures[12]. In contrast to conventional entropy alloys, there is also a strengthening mechanism through γ' precipitates with $L1_2$ phase but with good strength without forming detrimental phases in high entropy superalloys[14]. Comparison between high entropy superalloy HESA-3 and conventional superalloy CM247LC shows that HESA-3 is lighter, cheaper,

* Corresponding author: tria_laksana@itb.ac.id

ductile, stronger, and has better oxidation resistance than CM247LC[15]. The design of high entropy superalloys that remain in the composition range of 5 at.% ≤ x ≤ 35 at.% limiting the growth of the volume fraction and solvus temperature of the γ' phase[16].

High entropy superalloys have great potential to replace superalloys in high temperatures applications[6,13,17,18]. The selection of elements is an essential concern as it affects production costs. The generally very high Ni composition of these alloys gives a new design challenge to balance alloy cost and performance. Using Fe to substitute for Ni as the alloy base can reduce costs and weight, increasing energy efficiency in using materials. Fe is an ideal low-cost element to add to the solid solution matrix as it can be a substitute for Ni[17]. However, adding Fe is also known to decrease the stability of the γ' phase. Besides Fe, metal-based elements commonly added for superalloy engineering include Al, Cr, and Co. FeNiCrAlCo, one of the high entropy alloys with a combination of elements proven to perform well for high-temperature applications[19, 20]. Research by Gwalani et al.[19] on $Al_{0.3}$CoFeCrNi and $Al_{0.3}$CoFeCrNi$_2$ alloys shows the presence of the primary γ+γ' microstructure ($L1_2$) and its stability over a wide temperature range. On the other hand, Cu has the potential to be used to replace the more expensive Co, Ti, Mo, and W. Research by Huang et al. showed that Cu in the high entropy alloy AlCrFeNiTiCu_x increased the formation of the FCC phase and ductility but decreased the microhardness of corrosion resistance and wear resistance[21].

There are still limited publications available for Fe-based high entropy alloys, so further research is needed involving a wide variety of alloying elements to lower the Ni composition for the lowest possible cost. In addition, elements such as Zr in small concentrations can be added to strengthen grain boundaries. Research by Qi et al. showed that adding Zr to HEA CoCrFeNiZr_x up to x = 0.25 increased the tensile strength up to four times but still maintained good ductility[22]. Adding Zr dopant is expected to increase the toughness to failure due to crawling at high temperatures, which is essential to study[23].

Many researchers studied various alloy composition variations to improve the precipitated γ' phase thermal stability and lower the stacking fault energy (SFE) of γ matrix. Low SFE promotes the formation of stacking faults and twin boundaries, resulting in strength and toughness at high temperatures. Research by Tian et al. showed a relationship of increasing creep resistance with decreasing SFE in nickel-based super alloys[24]. Stacking fault energy in alloys can be determined empirically through characterization tools such as TEM and XRD or by simulation through first-principles, molecular dynamics, and thermodynamic methods[25]. In addition, ductility is also an essential aspect of alloy design, so the elasticity properties of the material need to be taken into account. The elastic constant can predict various mechanical properties, such as elastic modulus, shear modulus, Poisson's ratio, and compression modulus.

Computational methods can be used to design alloys for various elements. Compared to the conventional trial-and-error experiments, this method can provide efficiency in the time and cost required to combine the alloy compositions. This study uses a computational approach for high entropy superalloy FeNiCrAlCo and FeNiCrAlCu by adjusting the elasticity constant and stacking fault energy using first-principles density functional theory (DFT) calculations. The adjustments were made by changing the alloying elements and the composition of the alloy to obtain good mechanical properties. This understanding is expected to be an important step in designing and developing new materials, especially high-entropy superalloys.

2 Computational Procedure

The simulation was conducted in the first-principles DFT calculation framework using Cambridge Sequential Total Energy Package (CASTEP)[26]. The generalized gradient approximation (GGA) in the Perdew-Burke Ernzerhof (PBE) describes the exchange-correlation function[27]. Ultrasoft-type pseudopotential from Vanderbilt describes the nuclei and electron interaction and improves calculation efficiency. A plane-wave cut-off energy of 400 eV was used. These simulation parameters are basic approximations used in this study to approximate lattice parameters, elastic constant, SFE, and electronic structure.

2.1 Lattice Parameter and Elasticity Calculation

Lattice parameters as structural properties were calculated by partial relaxation of unit cell volume to achieve electronic minimization and by full relaxation of unit cell volume and shape. At the same time, the internal atomic positions changed to achieve electronic minimization and ionic minimization. The convergence criteria for electronic minimization and ionic minimization were set respectively at 2 x 10^{-5} eV/atom, and ionic Hellmann-Feynman force at 0.03 eV/Å. Based on the convergence test, the number of Monkhorst-Pack scheme k-points grid sampling is 18 irreducible k-points (6 x 6 x 1) FeNiCrAlCo and FeNiCrAlCu are assumed to have face-centered cubic (FCC) structures based on theoretical and experimental studies. The equilibrium lattice parameter of the 1 x 1 x 4 supercell with 24 atoms was obtained using the Birch-Murnaghan equation of states [28].

The elasticity constant is calculated on an optimized fcc unit cell measuring 1 x 1 x 2 with 8 atoms. The tolerances used include a maximum energy difference of 4 x 10^{-6} eV/atom, an ionic Hellmann-Feynman force of 0.01 eV/Å, and an ionic displacement of 0.01 Å. Based on convergence tests, the Monkhorst-Pack scheme k-points grid sampling is 6 x 6 x 3. Calculation of mechanical properties, such as compression modulus, shear modulus, elastic modulus, anisotropy, and the Poisson's ratio was carried out by the Voigt-Reuss-Hill approximation using Equations 3.2 to 3.8[29].

$$B_V = B_R = (C_{11} + 2C_{12}) \quad (1)$$
$$G_V = (C_{11} - C_{12} + 3C_{44}) / 5 \quad (2)$$
$$G_R = 5(C_{11} - C_{12})C_{44} / [4C_{44} + 3(C_{11} - C_{12})] \quad (3)$$
$$B = (B_V + B_R) / 2 \quad (4)$$
$$G = (G_V + G_R) / 2 \quad (5)$$
$$E = 9BG / (3B + G) \quad (6)$$
$$v = (3B-2G) / (6B+2G) \quad (7)$$

where B is bulk modulus, B_V is Voigt bulk modulus kompresi, B_R is Reuss bulk modulus, G is shear modulus, G_V is Voigt shear modulus, G_R is Reuss shear modulus, E is Young Modulus, dan v is Poisson ratio.

2.2 Stacking Fault Energy Calculation

The first-principles calculation to determine the SFE is performed by infinitely iterating the supercell structure with periodic boundary conditions. The FCC 1 x 1 x 4 supercell is composed in the [11-2], [-110], and [111] directions. This structure consists of 24 atoms with 12 layers that have a stacking order of ABCABCABCABC on a close-packed plane (111). To avoid interperiodic interactions in the [111] direction due to the repetition of periodic boundary conditions, the supercell structure is separated from the others by adding a vacuum of 10 Å.

The stacking fault structure was obtained by shifting the supercell in the (111) plane in the [11-2] slip direction. The shift is performed starting from the 7th to the 12th layer with a distance as far as $b_2 = a/6$[11-2] so that the supercell configuration becomes ABCABC][BCABCA which indicates the formation of HCP nuclei with BCBC arrangement in the FCC matrix. The first-principles calculation of the SFE (γ_{sf}) is performed based on the supercell method;

$$\gamma_{sf} = (E_{sf} - E_0) / A \quad (8)$$

E_{sf} is the total energy of the supercell with stacking fault, E_0 is the total energy of the perfect FCC structure without stacking fault, and A is the area of the stacking fault plane that depends on the equilibrium lattice parameter of the supercell, a_0.

In the SFE calculation, the placement of the combining elements in the supercell is one of the essential factors. The position of the supercell combining element is orderly based on the Suzuki segregation effect[30]. To study the effect of different compositions, one atom of Co, Ni, Al and Zr atoms are placed in the area around the stacking fault (layer 5) concerning the Suzuki segregation effect, as shown Fig. 1. The effect of Cu and Zr on the GSFE of this high entropy super alloy is known by variations of Cu and Zr at 4.17 and 8.33 at.%, and 0 and 4.17 at.% respectively. To find out the effect of Zr placement on the SFE, various structures with Zr that substituted Fe were compared.

3 Results and Discussion

3.1 Effect of Alloying Compositions on Lattice Parameter

The lattice parameter of FCC supercell 1 x 1 x 4 structure of FeNiCrAlCo was calculated by partial relaxation using Birch-Murnaghan's parameters in the EOS equation, as shown in Table 1. A full relaxation was conducted using CASTEP geometry optimization feature. The equilibrium lattice parameter from partial relaxation is 3.550 Å and from full relaxation is 3.552 Å, respectively. These lattice parameters are not much different from those obtained by Liang, F. et al. (3.541 Å) for the HEA AlCoCrFeNi structure prepared by the special quasi-random method[31], as well as those obtained through XRD by Fourmont et al. (3.530 Å) for FCC HEA AlCoCrFeNi[32]. The difference in the lattice parameters obtained is due to the difference in simulation accuracy and alloy composition. The partial relaxation method applies electronic minimization, resulting in an equilibrium lattice parameter corresponding to the lowest energy level at a fixed atomic position. On the other hand, the full relaxation method has a higher accuracy because it applies electronic minimization to determine the lowest energy level and ionic minimization, which is a relaxation of atomic positions and unit cells that results in the resultant force between atoms close to zero.

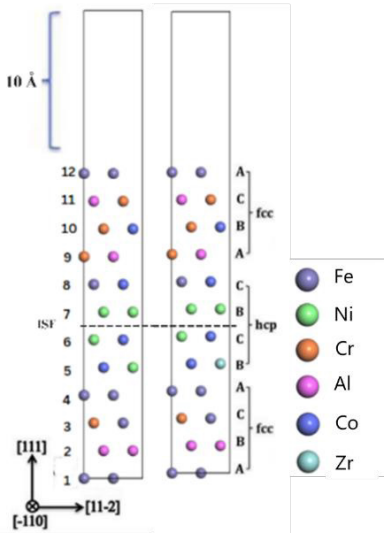

Fig. 1. Supercell structure of FeNiCrAlCo with intrinsic stacking fault (ISF) and Zr addition in the layer 5.

Adding Cu and Zr atoms can disrupt the local matrix environment so that the lattice expansion and the mechanical properties of the Fe-based high entropy superalloy FeNiCrAl can be affected. An increase in Cu concentration of 4.17 at.% increased the lattice parameters from 3.56 Å to 3.57 Å while the addition of 4.17 at.% Zr increased the lattice parameters from 3.57 Å to 3.63 Å. These results slightly differ from those of Borkar et al. using XRD, which showed that the $AlCrCuFeNi_2$ lattice parameter was 3.618 Å[33].

Table 1. Calculated lattice parameter of the FeNiCrAlCo and FeNiCrAlCu high entropy superalloy from first-principle calculation

Alloy	Lattice Parameter (Å)	Reference
$Fe_2NiCrAlCo$ (HESA)	3.550	This work
AlCoCrFeNi (HEA)	3.541	[31]
AlCoCrFeNi (HEA)	3.530	[32]
$Fe_2Ni_{(1-x)}CrAlCo+Zr_x$ (HESA)	3.608	This work
$Fe_{37}NiCrAlCu_4$ (HESA)	3.560	This work
$AlCrCuFeNi_2$ (HEA)	3.618	[33]
$Fe_{33}NiCrAlCu_8$ (HESA)	3.570	This work
$Fe_{33}NiCrAlCu_8+Zr$ (HESA)	3.630	This work

After optimization of the geometry, the atoms are relaxed in the [111] direction so that the spacing between layers can increase or decrease at a fixed volume at the elemental substitution sites. Fig. 2(a) shows the increasing distance between layers in layers 4-5 which Ni atom substituted for Zr. Decreasing Ni concentration accompanied by adding Zr in the alloy structure can increase the lattice parameter, partly because the radius of Zr atom (1.6 Å) is larger than the radius of Ni atom (1.24 Å). The substitution of Ni atoms with the Zr atom in the $Fe_2NiCrAlCo$ supercell lattice can cause the distortion of the local lattice. These are characterized by the increased distance between layers, especially between layers 4 and 5, which is the atom substitution position, from 2.06 Å to 2.16 Å, as shown in Fig. 2(a). This local lattice distortion is one of the causes of increasing the lattice parameters. This result is in accordance with the research by Vlasák et al.[34] which shows that the increase in the atomic radius of the alloy is directly proportional to the increase in the lattice parameter of the refractory HEA HfNbTaTiVZr.

Fig. 2(b) shows the increasing distance between layers in the area around Fe atom substituted for Cu and Zr, especially in layers 4-5. An increase in Cu concentration of 4.17 at.% increased the distance between layers from 1.97 Å to 2.03 Å, while the addition of Zr of 4.17 at.% increased the distance between layers from 2.03 Å to 2.49 Å. The effect of adding Zr to the distance between layers is greater than that of Cu because the Zr atomic radius reaches 1.6 Å, larger than Cu atoms of 1.286 Å and substituted Fe atoms of 1.228 Å. Increasing the lattice parameters and spacing between layers in the alloy geometry can cause lattice distortion. Molecular dynamic simulation by Wang et al. demonstrated that severe lattice distortion in AlCrCuFeNi alloy enhances the nucleation of dislocations but inhibits dislocation movement[10]. Increased dislocation density causes increased work hardening due to interactions between dislocations and atoms and good plasticity due to a more active slip system[10]. Increasing the distance between layers in the alloy geometry can also influence the strength of electronic bonds in the nearest neighbor and near the stacking fault area so that the SFE decrease[25].

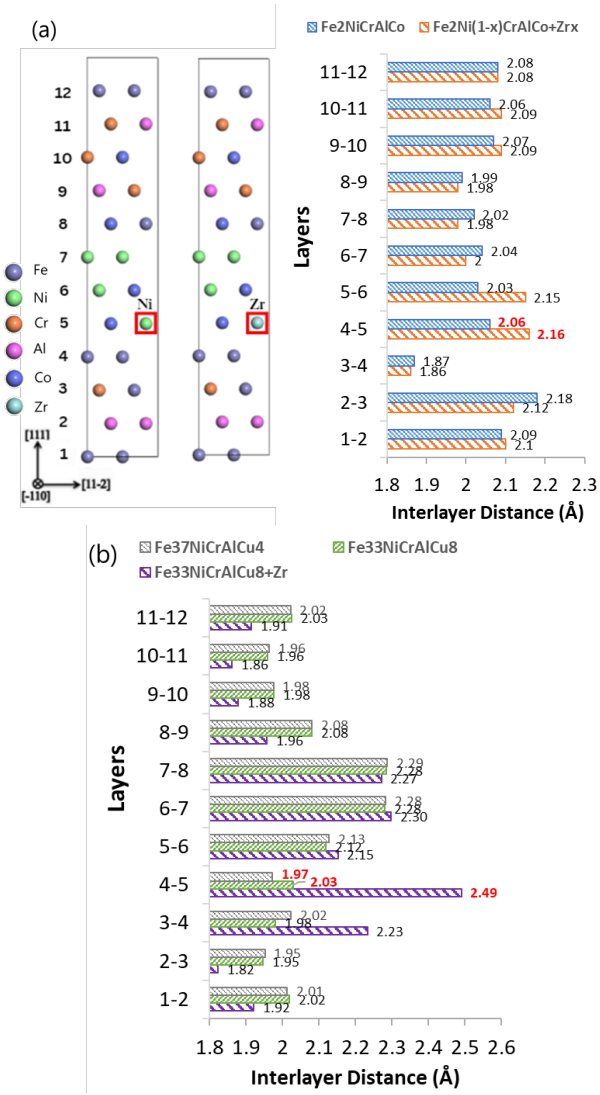

Fig. 2. Comparison of the calculated interlayer distance of (a) FeNiCrAlCo and (b) FeNiCrAlCu high entropy superalloy from first-principle calculation.

3.2 Effect of Alloying Compositions on Elasticity

Elastic constants describe the elastic properties of an alloy. For solid materials in general, elasticity constants consist of elastic constant (C_{ij}), Young's modulus, shear modulus, compression modulus, and Poisson's ratio[35]. The elastic constant in cubic crystals consists of C_{11}, C_{12}, and C_{44}, shown in Fig. 3, representing resistance to different deformation modes. The elastic constants C_{11}, C_{12}, and C_{44} of pure Fe and FeNiCrAlCo at the reduction of Ni concentration by 12.5 at.% and the addition of Zr with the same concentration are shown in Fig. 3(a). The reduction of Ni concentration and addition of Zr decreased the values of C_{11} and C_{44}, while C_{12} increased. This decreases resistance to tensile and compressive stresses in the [100] direction and shear stresses in the [110] direction. In comparison, resistance to shear

stresses in the [100] direction increases. Furthermore, the Cauchy pressure parameter (C_{12}-C_{44}) is positive, indicating that the reduction of Ni concentration and the addition of Zr increase the bonding strength of the metals in the alloy.

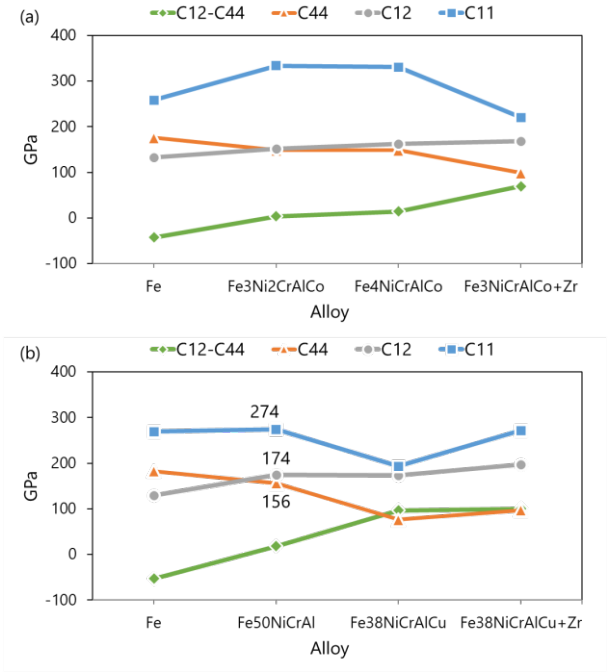

Fig. 3. Effect of alloying compositions on the calculated elastic constant of (a) FeNiCrAlCo and (b) FeNiCrAlCu high entropy superalloy from first-principle calculation.

In relation to the FCC structure, the mechanical stability review was also conducted based on the following Born-Huang elastic stability criteria[36]:

$$C_{11} - C_{12} > 0,\ C_{11} + 2C_{12} > 0, \text{ and } C_{44} > 0 \quad (9)$$

Based on this criterion, decreasing the Ni concentration by 12.5 at.% and adding Zr by 12.5 at.% to the FeNiCrAlCo HESA structure results in structural durability when subjected to mechanical loads, and has a lower risk of failure or deformation as indicated by the fulfillment of these criteria.

Fig. 3(b) shows that $Fe_{50}NiCrAl$ has C_{11}, C_{12}, and C_{44} values of 274 GPa, 174 GPa, and 156 GPa, respectively. This result is similar to the C_{11}, C_{12}, and C_{44} values of the first-principles simulation by Zuo et al. in the $Al_{0.05}CrFeNi$ alloy, which has a value of 240 GPa, 117 GPa, and 185 GPa, respectively[37]. The addition of Cu to the alloy as much as 12.5 at.% decreased C_{11}, C_{12}, and C_{44}, while the addition of Zr as much as 12.5 at.% to the alloy increased C_{11}, C_{12}, and C_{44}. This result shows resistance to [100] tensile and compressive stresses, [100] directional shear stresses, and [110] directional shear stresses, which decrease with the addition of Cu and vice versa increase with the addition of Zr. Adding Cu and Zr increases the Cauchy pressure, and the value is always positive (C_{12} - C_{44} > 0). This indicates a metallic bond that gets stronger with adding Cu and Zr.

Using the elastic constants obtained from first-principles calculation, the values of compression modulus (B), shear modulus (G), and Young modulus (E) were calculated with the Voigt-Reuss-Hill equation. The compression modulus (B) value represents the alloy's ability to resist volume deformation by external compressive forces, the shear modulus (G) represents the alloy's resistance to deformation by shear forces, and the Young modulus (E) represents the alloy's resistance to compressive or tensile forces in the elastic limit and a representation of the alloy's stiffness. Fig. 4(a) shows that the $Fe_3Ni_2CrAlCo$ structure, which is the initial structure, has a compression modulus (B), shear modulus (G), and Young modulus (E) of 213 GPa, 52 GPa, and 144 GPa, respectively. These values are close to the results obtained by Xiong et al.[38] from nano-indentation of HEA $AlCoCrFeNi_{2.1}$, which shows a shear modulus of 67.63 GPa and Young's modulus of 169.07 GPa. Decreasing the Ni concentration by 12.5 at.% caused an increase in compression modulus, shear modulus, and Young modulus with final values of 219 GPa, 118 GPa, and 300 GPa, respectively. The same trend of increasing towards decreasing Ni concentration was also evidenced in a study by Liu et al.[39] with CoCrFeNi HEA.

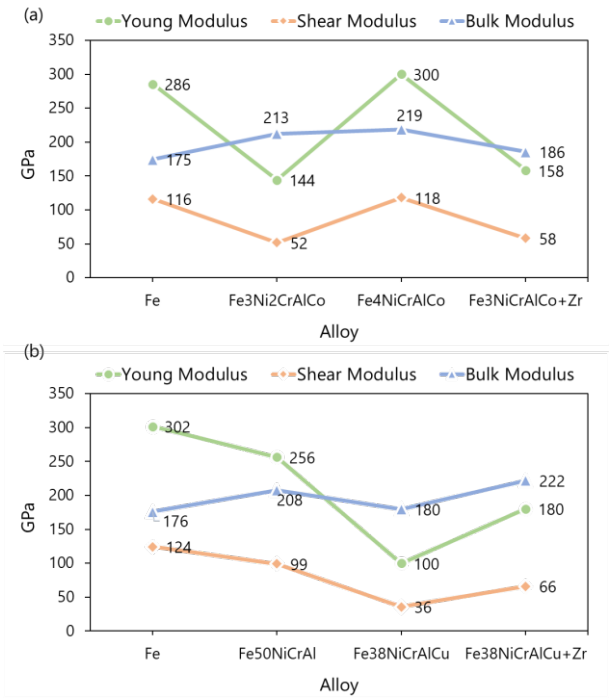

Fig. 4. Effect of alloying compositions on the compression modulus (B), shear modulus (G), and Young modulus (E) of (a) FeNiCrAlCo and (b) FeNiCrAlCu high entropy superalloy from first-principle calculation.

On the other hand, the addition of 12.5 at.% Zr causes an increase in shear modulus and Young modulus. Still, the compression modulus decreases with the final values of compression modulus, shear modulus, and Young modulus of 185.61 GPa, 58.32 GPa, and 158.36 GPa. Research by Ji et al.[40] on HEA TiTaNbZr for the variation of Zr addition of 5 at.% and research by Zhang et al.[41] on HEA CoCrFeNiMn with the addition of Zr around 4 at.% showed the same pattern of increase and decreased as this study, the value

of compression modulus, B, decreased, while G and E increased with the addition of Zr. Decreasing Ni concentration increases the ductility, resistance to forces in the shear direction, and resistance to forces in the compressive direction or resistance to deformation in each force direction. On the other hand, adding Zr tends to increase ductility and resistance to forces in the shear direction but decreases the resistance to forces in the compressive direction or deformation in certain directions of force.

Fig. 4(b) shows the shear, compression and elasticity modulus values of $Fe_{50}NiCrAl$ of 99 GPa, 208 GPa, and 256 GPa, respectively. This value can be compared with the first-principles simulation by Wang et al., which shows bulk, shear, and elasticity modulus of $Al_{0,3}CoLa_{0,1}NiFe0.6Cr_{0,6}$ for 54.96 GPa, 168.48 GPa, dan 148.7 GPa respectively[42]. Fig. 4(b) also indicates that the addition of 12.5 at.% Cu to the alloy decreases the shear modulus, compression, and elasticity. This shows the effect of adding Cu lowers the resistance to stress, resistance to compression, and stiffness. These results are in accordance with research by Liu et al. with nano-indentation testing, which showed that adding Cu decreased the Young's modulus of $Ti_{19}Zr_{19}Hf_{19}Nb_{19}Be_{19}$ HEA[43]. The addition of 12.5 at.% Zr to the alloy increases the compression modulus significantly until it almost reaches the compression modulus in the alloy without Cu and Zr. This differs from the study by Ji et al., which shows the addition of Zr lowers the compression modulus on HEA Ti-Ta-Nb-Zr. The difference in the effect of Cu and Zr is expected to positively affect the balance in the mechanical properties of the alloy.

Fig. 5(a) shows that decreasing the Ni concentration to 12.5 at.% increases the Zener ratio from 1.63 to 1.77 but decreases the Pugh ratio (B/G) from 4.09 to 1.85 and the Poisson ratio from 0.39 to 0.27. The increased Zener ratio indicates increased anisotropy, so the (100) and (110) planes have different physical properties. The decreased Pugh ratio (B/G) indicates decreased ductility, but since the value is > 1.75, it is still in the ductile category because it has not entered the transition to brittle. The decreased Poisson ratio indicates decreased shear stability and plasticity. On the other hand, the addition of 12.5 at.% Zr to the alloy increased the Zener ratio to 3.73 but decreased the B/G ratio to 3.18 and the Poisson ratio to 0.36. The Pugh (B/G) ratio in this variation has lowered but is still high, above 1.75, indicating the alloy has not yet transitioned to brittle and its excellent ductility. The decreased Poisson ratio indicates decreased shear stability and plasticity. Research by Zhang et al.[31] with CoCrFeNiMn alloys is consistent with this study that the addition of Zr resulted in a decrease in ductility as the Zr concentration increased. The percent elongation decreased from > 40% to 12% at a Zr concentration of about 20 at.%.

Fig. 5(b) shows that the addition of 12.5 at.% Cu to the alloy increased the Zener ratio from 3.13 to 7.51, the B/G ratio from 2.1 to 5.06, the Poisson ratio in the [001] direction from 0.39 to 0.47, and the Poisson's ratio in the [111] direction from 0.2 to 0.31. An increase in the Zener ratio indicates an increase in anisotropy so that the planes (100) and (110) have different physical properties. An increase in Pugh (B/G) ratio indicates an increase in ductility. In contrast, increasing Poisson's ratio indicates good shear stability and plasticity. On the other hand, the addition of 12.5 at.% Zr to the alloy decreases the Zener ratio, (B/G) ratio, anisotropy, and Poisson's ratio in the [001] and [111] directions. The Pugh ratio (B/G) value of 2.63 above 1.75 indicates that the alloy has not entered the ductile-brittle transition [29]. The Poisson ratio, which still reaches 0.42 and 0.31 in the [001] and [111] directions, respectively, also indicates that the material can withstand permanent/non-reversible deformation when subjected to stress. As a comparison, the $Al_{0.3}CoLa_{0.1}NiFe_{0.6}Cr_{0,6}$ alloy studied by Wang et al. showed the Zener ratio, B/G ratio, Poisson ratio [001], and [111] directions of 1.537, 3.066, 0.384 and 0.328 respectively[42]. This parameter can be a concern in the use of high entropy superalloys when receiving loading at high temperatures.

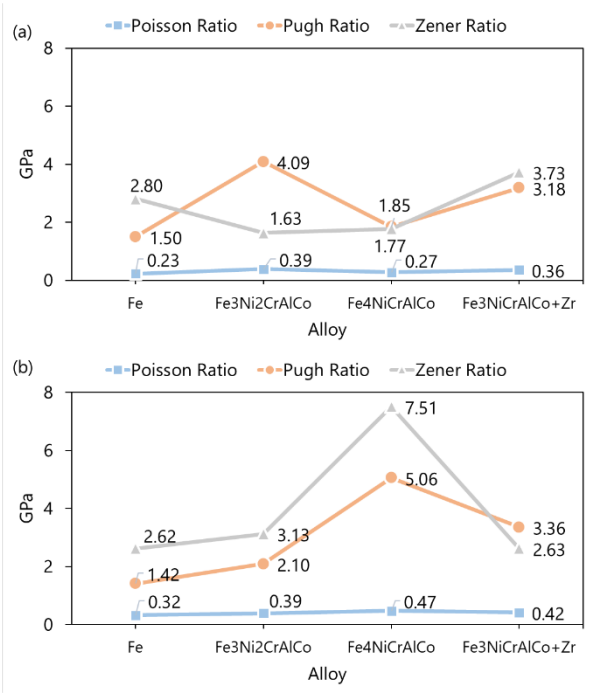

Fig. 5. Effect of alloying compositions on Poisson, Pugh, and Zener ratio of (a) FeNiCrAlCo and (b) FeNiCrAlCu high entropy superalloy from first-principle calculation.

3.3 Effect of Alloying Compositions on Stacking Fault Energy

The effect of composition variations on the SFE of FeNiCrAlCo is shown in Fig. 6. It is known that the $Fe_2NiCrAlCo$ alloy has an SFE of 0.135 J/m^2. A decrease in Ni concentration by 4.17 at.% accompanied by an increase in Fe and Co concentration by 4.17 at.% resulted in a reduction of the SFE value to 0.124 J/m^2 and 0.130 J/m^2, respectively. On the other hand, a decrease in Ni concentration accompanied by an increase in Cr concentration and the addition of Zr resulted in a significant reduction of the SFE to 0.107 J/m^2 and 0.089 J/m^2, respectively. However, the decrease in Ni concentration accompanied by an

increase in Al concentration resulted in a significant rise of the SFE to 0.162 J/m^2. The reduction of SFE is sequentially shown in the variation of Zr increase > Cr increase > Fe increase > Co increase > Al increase.

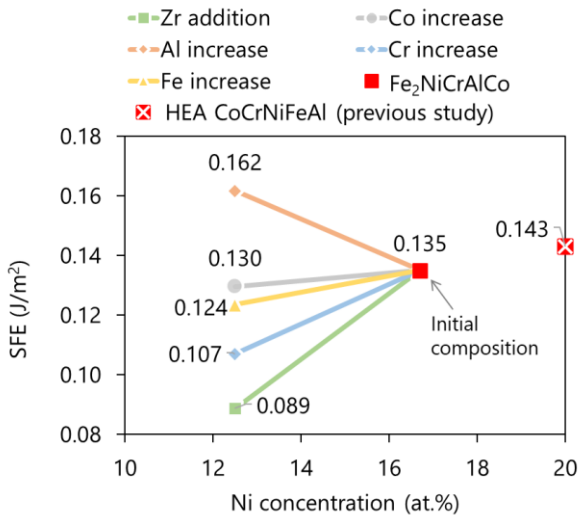

Fig. 6. Effect of alloying compositions on the SFE of high entropy superalloy FeNiCrAlCo from first-principle calculation.

Decreasing the Ni concentration by 4.17 at.% reduces the SFE. The highest SFE was obtained when increasing the Al concentration by 4.17 at.%, and the lowest SFE was obtained by adding Zr by 4.17 at.%. The results compared to the SFE of Murtadho, who used HEA CoCrFeNiAl with equiatomic composition (20 at.% Ni), showed a value of 0.143 J/m^2 where this value is higher than the SFE in this work, and also with a higher Ni concentration showing an increase in the SFE [44]. In addition, it was found that increasing Cr concentration caused the SFE to decrease while increasing Al concentration increased the SFE. Regarding the effect of Fe and Co, there is a difference with the previous results, which shows that the increased Fe and Co contribute to increasing SFE, but this can be understood because the decrease in these two elements is accompanied by a reduction of Cr concentration which causes a significant increase in SFE.

Fig. 7 shows the addition of Cu and an increase in Cu concentration of 4.17 at.% increases the SFE of high entropy superalloy FeNiCrAlCu. The increase in the SFE is in accordance with the study by Peng et al., which showed that the addition of Cu to TWIP Fe-20Mn-xCu-1.3C steel up to x = 3 increased the SFE to 0.03 J/m^2 so that the twinning mechanism was inhibited [45]. On the other hand, the addition of 4.17 at.% Zr to $Fe_{33}NiCrAlCu_8$ lowered the SFE from 0.151 J/m^2 to 0.139 J/m^2.

The stacking fault energy is influenced by various factors, including local lattice distortion and solid solution FCC phase stability[46]. Local lattice distortion tends to decrease the SFE value because it makes HCP nucleation easier to occur. On the other hand, a decrease in FCC phase stability increases the tendency for the transformation from FCC to HCP to occur and decreases the SFE. Based on this, a reduction in Ni concentration causes destabilization of the FCC phase and thus decreases the SFE. Increasing Co can play a role in increasing the stability of the HCP phase, which tends to cause a decrease in SFE. An increase in Cr and Zr concentrations causes destabilization of the FCC phase resulting in a reduction of the SFE. Meanwhile, increasing Al generally causes a decrease in the stability of the FCC phase, but in this study, an increase in the SFE was obtained. The rise of SFE by increasing Al can be caused by the nature of the element Al, which has a very high SFE (> 0.25 J/m^2), contributing to the increased SFE significantly. Based on the lattice parameters, the SFE is relatively consistent with the increase of the lattice parameters and in the distance between layers with decreasing Ni and adding Zr.

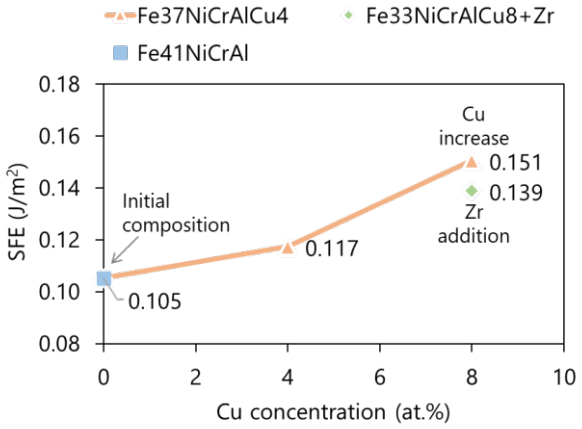

Fig. 7. Effect of Cu and Zr concentrations on the SFE of high entropy superalloy FeNiCrAlCu from first-principle calculation.

To determine the effect of atom placement on the SFE, Zr atoms that substitute Fe are placed in layers 1, 2, 3, 4, 9, 10, 11, and 12. Fig. 8 shows the relatively constant value of SFE at different atomic placements. However, in layer 9, SFE drops to 0.08 J/m^2 due to the interaction of the Zr atom with the surrounding atoms, especially with Al atom. The differences in SFE at the various Zr atom location are in accordance with the study by Wen et al., which shows that there is a difference in lattice distortion produced by Zr atoms when placed in the stacking fault area and FCC planes of Co and Ni alloys so that the SFE is different[47].

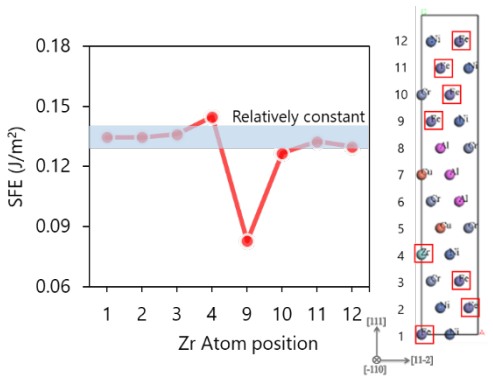

Fig. 8. Effect Zr atom position on the SFE of high entropy superalloy FeNiCrAlCu.

3.4 Effect of Alloying Compositions on Electronic Structure

The strength of the electronic bonds in nearby atoms and around the stacking fault can affect the SFE and other mechanical properties. Electronic structure analysis was carried out to determine the effect of decreasing and adding Zr to Fe-based high entropy superalloys by analyzing the density of states (DOS) and charge density difference.

3.4.1 Density of States

To gain in-depth knowledge of the electronic properties of the alloy during shearing, the density of states (DOS) is analyzed to obtain a visual picture of the bond energy structure. DOS defines the number of states at each energy level available for an electron to occupy. The DOS value at the Fermi energy point (0 eV) is analyzed because it correlates with electronic bonding in a structure. The total DOS of the Fe-based high entropy superalloys FeNiCrAlCo with the variations of compositions are presented in Fig. 9. Around the Fermi energy, the peak of the total DOS is dominated by the *d* shell. The electronic configurations of the Cr and Zr valence shells are $3d^5\ 4s^1$ and $4d^2\ 5s^2$, respectively. Meanwhile, the electronic configurations of Fe, Ni, Al, and Co are $3d^6\ 4s^2$, $3d^8\ 4s^2$, $3s^2\ 3p^1$, and $3d^6\ 4s^2$, respectively. The decrease in Ni concentration by 4.17 at.% tends to decrease the total DOS value at the Fermi energy position. The reduction in total DOS value is characterized by the initial structure with high Ni concentration (16.67 at.%) having the highest total DOS value. With a change in composition, the total DOS value changes towards the initial structure due to the distribution of electrons, which can change the atomic bonds in a structure. Based on this, a decrease in Ni concentration of 4.17 at.% causes a decrease in the strength of atomic bonds and tends to decrease the SFE value. Similarly, adding Zr causes a decrease in total DOS and leads to a reduction of SFE. More specifically, the total DOS decreases in the order of; Al increase > Cr increase > Zr increase > Fe increase > Co increase > initial structure.

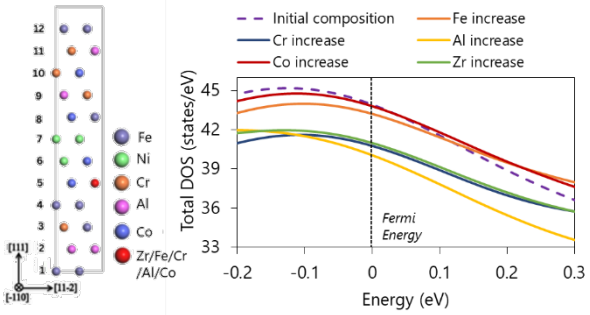

Fig. 9. Total DOS of $Fe_{33}Ni_{16.7}CrAlCo$ (initial composition) and the effect of the increase in concentration by 4.17 at.% for elements Fe, Cr, Al, Co, and Zr.

3.4.2 Charge Density Difference

When alloying atoms are added to the alloy matrix, changes in the charge density distribution and bonding will occur to achieve a neutral charge state. Therefore, physical analysis can be carried out so that the causes of changes in mechanical properties can be better known. The effect of the distribution of charge density can be seen through the contours of the difference in charge density in units of $\delta\rho/Å^3$ on the slice representing the plane in the [11-2] and [111] directions, as shown in Fig. 10. On the contour scale used, the red and yellow colors indicate positive values indicating charge accumulation, while the blue and green colors indicate negative values indicating charge depletion.

Fig. 10(a) shows the initial structure with a Ni concentration of 16.7 at.% resulted in a red charge accumulation zone of 22.26% and 42.63%, while green and blue charge depletion zones of 18.56% and 16.55%, respectively. Among each variation, the decrease in Ni concentration by 4.17 at.% accompanied by an increase in Cr and Zr showed the highest increase in the red accumulation zone to 24.97% and 22.92%, respectively, as shown in Fig. 10(c) and Fig. 10(f). The increase is directly proportional to the analysis results of total DOS and a significant decrease in SFE. Fig. 10(b) and Fig. 10(e) show that a decrease in Ni concentration by 4.17 at.% accompanied by an increase in Fe and Co concentration, the red charge accumulation zone tends to decrease to 22.09% and 21.98%, respectively, but the yellow accumulation zone increases to 43.52% and 43.18% respectively. This also shows an increasing trend of the charge accumulation zone, which is consistent with the results of the total DOS analysis, and a decrease in the SFE value. On the other hand, the decrease in Ni concentration accompanied by the increase in Al concentration shown in Fig. 10(d) resulted in the red accumulation zone dropping to 21.58%, the lowest percentage among the variations. This phenomenon is consistent with the effect of Al addition on the SFE, which shows an increase.

Theoretically, the larger charge accumulation area, especially around the stacking fault area, tends to decrease the SFE. The decrease in SFE is due to weakening of the metallic bond strength in the layer around the SF formation site. This is proven by the analysis results shown in Fig. 10 where the area of the red charge accumulation area can be sorted into; Cr increase > Zr increase > initial structure > Fe increase > Co increase > Al increase, which is relatively consistent with the sequence of SFE and analysis of DOS. Based on these results, it is known that decreasing Ni concentration and adding Zr tends to increase the charge accumulation zone.

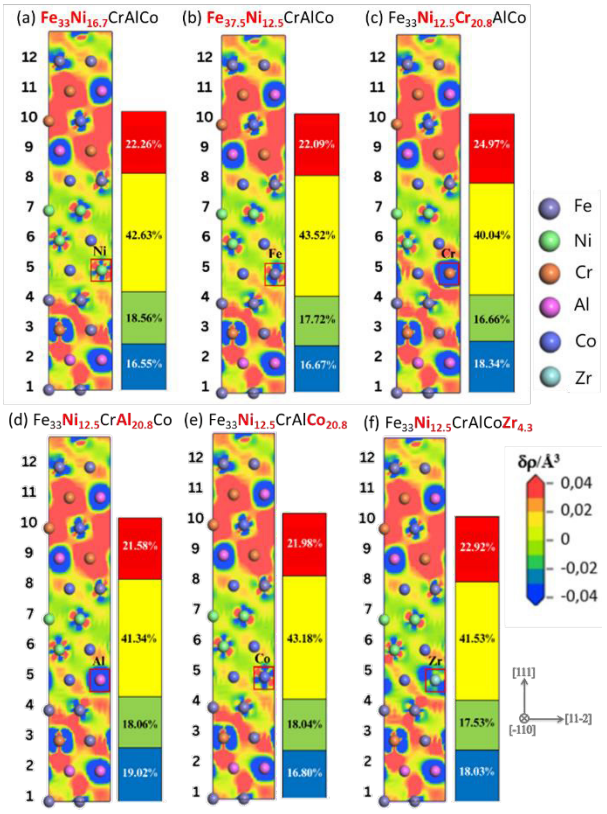

Fig. 10. Charge density difference of (a) $Fe_{33}Ni_{16.7}CrAlCo$, and the effect of the increase in concentration by 4.17 at.% for elements (b) Fe, (c) Cr, (d) Al, (e) Co, and (f) Zr.

3.5 Designing Fe-based High Entropy Superalloy FeNiCrAlCo and FeNiCrAlCo for High Temperature Applications

To provide a clear picture, the effect of Ni reduction and Zr addition to HESA FeNiCrAlCo and adding Cu and Zr to HESA FeNiCrAlCu on the elasticity properties and the SFE are summarized in Table 2. High entropy superalloys present challenges that reduce their preference for use, including a tendency to be brittle over a wide temperature range, excessively high hardness, and relatively high cost. In addition, designing high entropy superalloys for high temperatures applications is produced by tailoring the compositions to have a low SFE and obtain a specific deformation mechanism. Therefore, an assessment was made based on the tendency of deformation mechanisms that can occur in Fe-based HESA and some essential criteria in high temperature performance, such as elasticity, ductility, and material cost.

Table 2 shows that decreasing Ni to 12.5 at.% tends to increase the elasticity properties and produce good ductility in HESA FeNiCrAlCo. Similarly, adding Zr to 12.5 at.% tends to increase the elasticity properties and produce excellent ductility in HESA FeNiCrAlCo. Good ductility is necessary to produce toughness over a wide temperature range in HESA FeNiCrAlCo that already have high strength as their primary property[15]. The decrease in Ni concentration by 4.17 at.% to the final concentration of 12.5 at.% and the addition of Zr by 4.17 at.% resulted in an increasing trend in lattice parameters and average interlayer distance, indicating the occurrence of local lattice distortion in the form of expansion. This local lattice distortion is directly proportional to the tendency of decreasing SFE. The partial dislocation deformation is an expected dominant deformation mechanism because it can increase stacking fault formation and even form twin boundaries. Adding Zr resulted in the highest SFE reduction. Meanwhile, increasing the Cr concentration resulted in the second-highest decrease in SFE. Increasing the Cu concentration and adding Zr to the HESA FeNiCrAlCo increases the lattice parameters so that the lattice is distorted. Adding Cu and Zr increased the ductility while reducing the strength.

Table 2. Summary of the effect of alloying composition on Lattice Parameters, strength, ductility, and SFE of High Entropy Superalloys from First Principles Calculations

Effect	Lattice Parameter	Strength	Ductility	SFE
1. HESA FeNiCrAlCo				
Decreasing Ni	-	⇩	⇧	⇩
Adding Zr	⇧	⇩	⇧	⇩
2. HESA FeNiCrAlCo				
Adding Cu	-	⇩	⇧	⇧
Increasing Cu Concentration	⇧	-	-	⇧
Adding Zr	⇧	⇧	⇩	⇩

Note: ⇧: increase, ⇩: decrease

Supported by the data obtained by Cui et al.[48] showed that increasing Cr with variations from 0.2y, 0.4y, and 0.6y (y = 3.3 wt.%) affects mechanical properties by increasing strength, hardness, and ductility. In terms of compression strength, the study shows that increasing the Cr concentration increases the strength from 1896 MPa at concentration 0.2y, to 3524 MPa at concentration 0.6y at room temperature. In addition, the variation of Cr and temperature also shows an increase in strain from 15.7% to 43.3% at 0.6y concentration, indicating an increase in ductility. Furthermore, it is also known that increasing the Cr concentration increases the strength and ductility at 800°C sequentially from about 375 MPa and 37% at 0.2y concentration to about 400 MPa and 47% at 0.6y concentration.

Fe-based super high entropy alloys used at high temperatures need to pay attention to creep resistance. Tian et al. have described the relationship between SFE and creep deformation mechanism at the creep stage[24]. This shows that adding Cu, which increases SFE, will affect the dominant mode in the secondary and tertiary creep stages to become isolated faults so that the dislocation slip increases in the matrix and the creep resistance decreases. The addition of Zr to the high entropy superalloy will make the micro-twin mode dominant in the second and third stages so that there is a twin boundary interaction with dislocations, increasing cross-slip resistance and creep strain rate[24]. This result concludes the increase in creep resistance with decreasing Ni concentration and adding Cu and Zr.

4 Conclusion

1. The decrease in Ni concentration followed by an increase in the other element, such as Cu, and the addition of Zr by 4.17 at.% in the HESA FeNiCrAlCo and FeNiCrAlCu will increase the equilibrium lattice parameter and the average interlayer distance. The increase in lattice parameters is due to differences in atomic size. Concerning the elasticity, adding Cu will increase the ductility, while adding Zr will increase the strength and slightly decrease the alloy's ductility. However, it is still in the ductile category because it has not yet transitioned to brittle.

2. The decrease in Ni concentration accompanied by the increase in Fe, Cr, Co, and Zr concentrations, decreased the SFE, while the increase in Al concentration increased the SFE. The decrease of SFE from the initial structure of $Fe_{33}Ni_{16.7}CrAlCo$ (0.135 J/m^2) is sequentially shown in the variation of Zr addition > Cr increase > Fe increase > Co increase > Al increase. The addition of Cu and an increase in Cu concentration from the initial structure of $Fe_{37}NiCrAlCu_4$ (0.105 J/m^2) increased the SFE to 0.117 and 0.151 J/m^2, while the addition of Zr.% reduced the SFE to 0.139 J/m^2. Decreasing the SFE of HESA will increase its strength but still have good ductility.

3. The change of SFE can be explained by the density of states and charge density difference. The increasing charge accumulation area can cause a decrease in the SFE. Therefore, the density of states at the Fermi energy decreases, the bonds between atoms become weaker, interatomic distance increases, and the stacking fault energy decreases.

4. HESA FeNiCrAlCo is predicted to have better strength than HESA FeNiCrAlCo due to the lower calculated SFE from first-principle calculations (SFE of $Fe_{33}Ni_{16.7}CrAlCo$ is 0.135 J/m^2 while SFE of $Fe_{33}Ni_{16.7}CrAlCu_8$ is 0.151 J/m^2). The Fe-based HESA design can be optimized by decreasing Ni concentration to decrease SFE, accompanied by increasing Cr concentration to decrease SFE to significantly increase strength, ductility, and hardness, especially at high temperature, or adding Zr to decrease SFE to the maximum. Other elements, such as Cu can be added to improve its ductility further.

Acknowledgments

This work was supported by the Research, Community Service, and Innovation (PPMI) Program ITB 2023, the Research Program ITB 2021 (FTTM.PN-6-17-2021) and Research and Innovation Program for Advanced Indonesia (RIIM) 2022 BRIN.

References

1. R.C. Reed, Roger C., *The superalloys : fundamentals and applications*, Cambridge University Press, (2006)
2. E.A. Basuki, D. H. Prajitno, F. Muhammad, *Alloys developed for high temperature applications*, in proceedings of AIP Conference, American Institute of Physics Inc., (2017)
3. R. Viswanathan, R. Stringer, *Failure mechanisms of high temperature components in power plants*, (2000)
4. P. Eliott, *A practical guide to high-temperature alloys*, Mat. And Des. Vol. **12**, 6, (1991)
5. M. Simić, A. Alil, S. Martinović, M. Vlahović, A. Savić, T.V. Husović, *High temperature materials: properties, demands, and applications,* Hem. Ind., **74**, 4. Association of Chemists and Chemical Engineers of Serbia, 273–284, (2020)
6. T. Tsao, *Developing new type of high temperature alloys–high entropy superalloys*, Int. J. of Metal. & Mater. Eng., **1**, 1, (2015)
7. J.B. Wahl, K. Harris, *CMSX-4® plus single Crystal alloy development, characterization and application development*, in proceedings of the International Symposium on Superalloys, Min. Metal. and Mater. Soc., 25-33, (2016)
8. J.-W. Yeh, Recent progress in high-entropy alloys, *Annales de Chimie Science des Matériaux* **31**, 633–648 (2006)
9. Y. Zhang, *Microstructures and properties of high-entropy alloys*, Prog. in Mater. Sci., **61**, 1–93, (2014)
10. L. Zhang, Y. Zhou , X. Jin, X. Du, B. Li, *The microstructure and high-temperature properties of novel nano precipitation-hardened face centered cubic high-entropy superalloys*. Scr Mater **146**, 226–230 (2018)
11. C.-M. Kuo, C.-W Tsai, *Effect of cellular structure on the mechanical property of Al0.2Co1.5CrFeNi1.5Ti0.3 high-entropy alloy*, Mater Chem Phys **210**, 103–110 (2018)
12. Y.-T. Chen, *Hierarchical microstructure strengthening in a single crystal high entropy superalloy*, Sci Rep **10**, 12163 (2020)
13. T.K. Tsao, *The high temperature tensile and creep behaviors of high entropy superalloy*, Sci. Rep., **7**, 1, (2017)
14. T. Tsao, *Developing New Type of High Temperature Alloys–High Entropy Superalloys*, International Journal of Metallurgical & Materials Engineering **1**, (2015)
15. Y.T. Chen, Y.J. Chang, H. Murakami, S. Gorsse, A.C. Yeh, *Designing high entropy superalloys for elevated temperature application*. *Scr Mater* **187**, 177–182 (2020)

16. M.C. Gao, J.W. Yeh, P.K. Liaw, Y. Zhang, *High-entropy alloys: Fundamentals and Application*, (2016)
17. Y.T. Chen, Y.J. Chang, H. Murakami, S. Gorsse, A.C. Yeh, *Designing high entropy superalloys for elevated temperature application*, Scr. Mater., **187**, 177–182, (2020)
18. S. El-Hadad, *High entropy alloys: the materials of future*, Int. J. of Mater. Tech. and Innov., **2**, 67–84, (2022)
19. B. Gwalani, *Stability of ordered $L1_2$ and B2 precipitates in face centered cubic based high entropy alloys - $Al_{0.3}$CoFeCrNi and $Al_{0.3}$CuFeCrNi2*, Scr. Mater., **123**, 130–134, (2016)
20. I.S. Wani, *Cold-rolling and recrystallization textures of a nano-lamellar AlCoCrFeNi$_{2.1}$ eutectic high entropy alloy*, Intermetal. (Barking), **84**, 42–51, (2017)
21. L. Huang, *Effect of Cu segregation on the phase transformation and properties of AlCrFeNiTiCux high-entropy alloys*, Intermetallics **140**, 107397 (2022)
22. W. Qi, *Effect of Zr on phase separation, mechanical and corrosion behavior of heterogeneous CoCrFeNiZr high-entropy alloy*, J Mater Sci Technol **109**, 76–85 (2022)
23. S. Brito-Garcia, J. Mirza-Rosca, V. Geanta, I. Voiculescu, *Mechanical and corrosion behavior of Zr-doped high-entropy alloy from CoCrFeMoNi System*, Mater., **16**, 5, (2023)
24. C. Tian, G. Han, C. Cui, X. Sun, *Effects of stacking fault energy on the creep behaviors of Ni-base superalloy*, Mater Des **64**, 316–323 (2014)
25. T.L. Achmad, W. Fu, H. Chen, C. Zhang, Z.-G. Yang, *First-principles calculations of generalized-stacking-fault-energy of Co-based alloys*, Comput Mater Sci **121**, 86–96 (2016)
26. S. J. Clark, M. D. Segall, C. J. Pickard, P. J. Hasnip, M. J. Probert, K. Refson, M. C. Payne*, First principles methods using CASTEP*, Z. Kristallogr., **220**, 567-570, (2005)
27. J.P. Perdew, K. Burke, M. Ernzerhof, *Generalized gradient approximation made simple*, Phys. Rev. **77**, 18, (1996)
28. X. Li, X. Chen, L. Han, C. Ruan, P. Lu, P. Guan, *First-principles study of the structural, elastic and electronic properties of Pt_3M alloys*, J. Mater. Res., **31**, (2016)
29. F. Birch, *Finite elastic strain of cubic crystal*, Phys. Rev., **71**, 809, (1947)
30. Wen, D., M.S. Titus, *First-principles study of suzuki segregation at stacking faults in disordered face-centered cubic Co-Ni alloys*, Act. Materia. (2021)
31. F. Liang, J. Du, G. Su, C. Xu, C. Zhang, X. Kong, *Phase stability and mechanical properties analysis of $AlCo_xCrFeNi$ HEAs based on first principles*, Metals (Basel), **12**, (2022)
32. A. Fourmont, et al. *Effects of mechanical activation on chemical homogeneity and contamination level in dual-phase AlCoCrFeNi high entropy alloy*, Mater. Chem. Phys., **272**, (2021)
33. T. Borkar, *A combinatorial assessment of AlxCrCuFeNi2 (0 < x < 1.5) complex concentrated alloys: Microstructure, microhardness, and magnetic properties*, Acta Mater **116**, 63–76 (2016)
34. T. Vlasák, et al., *Thermal stability of microstructure of high-entropy alloys based on refractory metals Hf, Nb, Ta, Ti, V, and Zr*, Metals (Basel), **12**, (2022)
35. H.M. Ledbetter, R.P. Reed, *Elastic properties of metals and alloys, I. iron, nickel, and iron-nickel alloys*, J. Phys. Chem. Ref. Data., **2**, 531–618, (1973)
36. M. Born, *On the stability of crystal lattices I*, Mathematical Proceedings of the Cambridge Philosophical Society, **36**, 160–172, (1940)
37. X. Zuo, N. Moelans, *Phase-field study of elastic effects on precipitate evolution in (Al)0.05CrFeNi*, Int J Mech Sci **247**, 108163 (2023)
38. T. Xiong, et al., *Faceted Kurdjumov-Sachs interface-induced slip continuity in the eutectic high-entropy alloy, AlCoCrFeNi$_{2.1}$*, J. Mater. Sci. Technol, **65**, 16–227, (2021)
39. H. Liu, C. Xin, L. Liu, C. Zhuang, *Effects of different contents of each component on the structural stability and mechanical properties of Co-Cr-Fe-Ni high-entropy alloys*, App. Sci. (Switzerland), **11**, (2021)
40. G. Ji, et al., *Effect of Zr addition on the local structure and mechanical properties of Ti–Ta–Nb–Zr refractory high-entropy alloys*, J. Mat. Res.Techno., **19**, 4428–4438, (2022)
41. H. Zhang, L. Zhang, X. Liu, Q. Chen, Y. Xu, *Effect of Zr addition on the microstructure and mechanical Properties of CoCrFeNiMn high-entropy Alloy synthesized by spark plasma sintering*, Entropy, **20**, (2018)
42. X. Wang, et al., *Effects of Al and La elements on mechanical properties of CoNiFe0.6Cr0.6 high-entropy alloys: a first-principles study*, Journal of Materials Research and Technology **23**, 1130–1140 (2023)
43. M. L. Liu, et al., *Ductilizing Ti19Zr19Hf19Nb19TM5Be19 (TM = Fe, Co, Ni and Cu) high-entropy bulk metallic glass composites via in-situ precipitated refractory high-entropy alloy dendrites*, *Intermetallics (Barking)* **152**, 107755 (2023)
44. M. Murthado, *Desain paduan entropi tinggi CoCrNiFeAl dan CoCrNiFeSi dengan Metode Perhitungan Termodinamika dan Simulasi First Principles*, (2022)
45. Peng, X. *et al.* Stacking fault energy and tensile deformation behavior of high-carbon twinning-induced plasticity steels: Effect of Cu addition. *Mater Des* **45**, 518–523 (2013).

46. H. Song, et al., *Local lattice distortion in high-entropy alloys*, Phys. Rev. Mater., **1**, (2017)
47. D. Wen, M.S. Titus, *Electronic origin of Suzuki segregation of transition metal elements in face-centered cubic Co and Ni alloys*, *Comput Mater Sci* **220**, 112033 (2023)
48. P. Cui, W. Wang, Z. Nong, Z. Lai, Y. Liu, J. Zhu, *Effects of Cr content on microstructure and mechanical properties of Co-free* $FeCr_yNiAl_{0.8}$ *high-entropy alloys*, Mater., **16**, 3348, (2023)